

Letter of Intent: Open Charm at JLab with the sPHENIX MAPS tracker

Miguel Arratia* and Sebouh J. Paul
University of California, Riverside

Yuri Gotra
Thomas Jefferson National Accelerator Facility

Hayk Hakobyan
Universidad Tecnica Federico Santa Maria, Valparaiso, Chile

Bryan McKinnon
University of Glasgow, Glasgow, United Kingdom
(Dated: May 8, 2024)

We propose a physics program at JLab with CLAS12 focusing on open-charm measurements, aiming to complement and expand current studies of J/ψ at (sub) threshold. This program will aid us in elucidating the J/ψ production mechanisms, which is crucial for interpreting data in terms of gluon form factors and offer potential insights into the intrinsic charm hypothesis and cold-nuclear matter effects. We discuss the technical feasibility of integrating the sPHENIX monolithic-active-pixel sensor (MAPS) tracker, known as MVTX, with the CLAS12 detector. The sPHENIX MVTX would support an open-charm program by providing excellent secondary-vertex performance for tagging D mesons. We study the kinematics of $\gamma p \rightarrow \bar{D}^0 \Lambda_c$ through phase-space simulations and estimate rates for the tagged quasi-photoproduction regime available with the CLAS12 forward tagger. While open-charm cross-sections at threshold remain uncertain, various predictions suggest that these measurements could be feasible when combined with conservative estimates of detector acceptance and luminosity. These preliminary estimates motivate detailed Geant detector simulations of signals and backgrounds, along with thorough technical assessments of operating conditions, to further explore the feasibility of these measurements in future dedicated CLAS12 experiments at JLab.

CONTENTS

I. Motivation for a Measurement of Open-Charm production at Threshold	2
II. Experimental Setup	3
A. The sPHENIX MAPS Vertex Tracker	4
B. Integration of the MVTX in CLAS12	4
C. Trigger rate, radiation tolerance, material budget	4
D. Triggering with the Forward Tracker	4
III. Observables and Analysis Methods	5
IV. Estimated Reach	6
A. Total expected cross section	6
B. Luminosity	6
C. Monte-Carlo Simulations	7
D. Estimation of efficiency and acceptance	7
E. Geometric acceptance of the MVTX	8
F. MVTX efficiency	8
G. Event retention after displaced-vertex cut	8
H. Expected sample size and reach	9
V. Summary and Conclusions	10
References	10

* Corresponding author: miguel.arratia@ucr.edu

I. MOTIVATION FOR A MEASUREMENT OF OPEN-CHARM PRODUCTION AT THRESHOLD

The study of J/ψ photoproduction at threshold has attracted considerable attention, with the objective of accessing the gluonic structure of the nucleon, and, ultimately, contributing to our understanding of the origin of the nucleon mass, see e.g Refs. [1–8]. This has motivated various experiments at JLab [9, 10], including GlueX at Hall-D [11, 12], the J/ψ -007 experiment at Hall-C [13], CLAS12 at Hall-B [14, 15], and SoLID at Hall-A [16].

The analysis of $\gamma p \rightarrow J/\psi p$ cross-section measurements typically relies on the assumption that the reaction mechanism can be described by the “vector-dominance model” (VDM) as illustrated in the left panel of Figure 1. Within this framework, the reaction is factorized into a hard $\gamma \rightarrow c\bar{c}$ vertex and a soft proton matrix element. Crucially, this factorization enables the extraction of the forward elastic-scattering amplitude of J/ψ off a proton, see e.g Ref. [17–20].

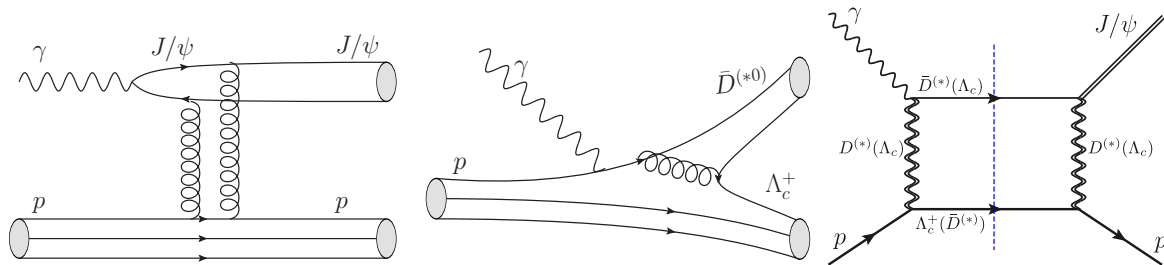


FIG. 1. Left: J/ψ production mechanism as per the vector-dominance model. Middle: Open-charm production mechanism. Right: J/ψ production mechanism through open-charm coupled channel suggested by Du *et al.* [21]. Source: Ref. [21].

Such assumptions have, however, been questioned, for example by Du *et al.* [21] who suggested that the reaction mechanism leading to the $J/\psi p$ final state could at least in part proceed through an open-charm coupled channel, illustrated in the right panel of Figure 1. In this model, open-charm production is followed by re-scattering of \bar{D} and Λ_c to produce the $J/\psi p$ final state. Note that the energy threshold for J/ψ photoproduction (≈ 8.2 GeV) is close to the threshold of the $\gamma p \rightarrow \bar{D}^0 \Lambda_c$ and $\gamma p \rightarrow \bar{D}^* \Lambda_c$ reactions (≈ 8.7 GeV and ≈ 9.4 GeV, respectively). This mechanism is not factorized like VDM and is not amenable to the interpretation of the $\gamma p \rightarrow J/\psi p$ data in relation to the gluonic structure of the nucleon.

The latest measurement of J/ψ at threshold by GlueX [12], shown in the left panel of Figure 2, revealed intriguing trends in the dataset near threshold, although with weak statistical significance (2.6σ). These features, not initially anticipated within the vector-dominance model, align with the open-charm mechanism proposed by Du *et al.*[21]. Notably, the cusp features appear at the threshold values for both $\gamma p \rightarrow \bar{D}^0 \Lambda_c$ and $\gamma p \rightarrow \bar{D}^* \Lambda_c$.

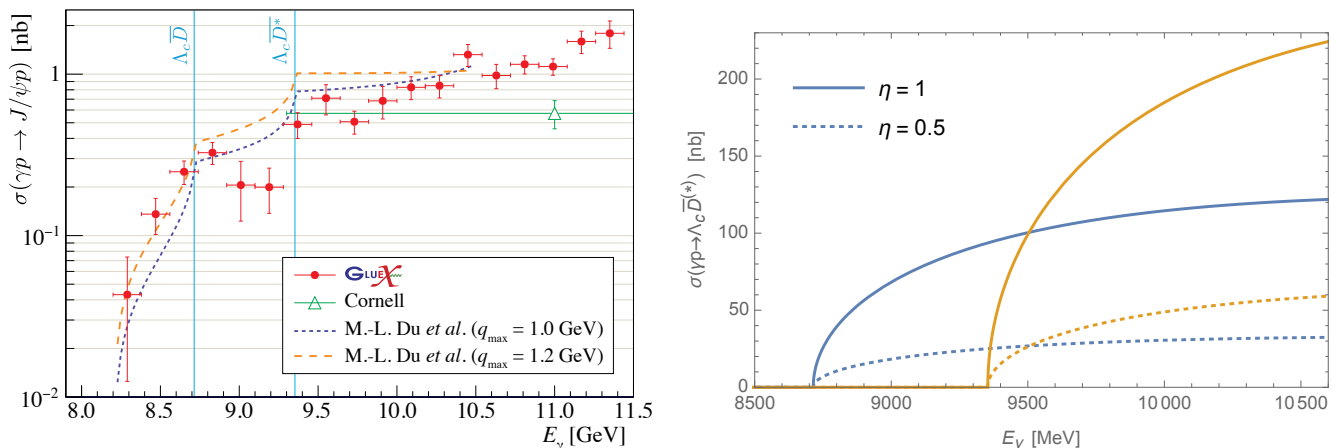


FIG. 2. Left: GlueX measured J/ψ photoproduction near the threshold, with vertical lines indicating the threshold energy for production of $\gamma p \rightarrow \bar{D}^0 \Lambda_c$ and $\gamma p \rightarrow \bar{D}^* \Lambda_c$. The curves represent predictions by Du *et al.* [21]. Source: Ref. [12]. Right: Du *et al.* predictions for open-charm production near the threshold, for $\Lambda_c^+ \bar{D}^0$ (blue) and $\Lambda_c^+ \bar{D}^{*0}$ (orange), indicating two scenarios depending on the model parameter η . Note how the open-charm cross-section is predicted to be one or two orders of magnitude higher than the J/ψ cross-section. Source: Ref. [21].

Another intriguing feature not expected in the VDM model was uncovered by the Hall-C experiment [13], which measured differential double-differential cross-sections as a function of the momentum transfer, t , and photon energy, E_γ . For the most part, the cross-section is well described by a falling exponential function in t , but some data present an upward trend at high t , which might be expected from u -channel exchange.

A partial-wave analysis carried out by the JPAC collaboration [22] suggests that both features—namely, the cusps in GlueX data and the upward trend in t in Hall-C data—are compatible with the open-charm coupled channel model, although with large statistical uncertainties. Thus far, the Du *et al.* model cannot be ruled out with existing experimental data, or as they put it: “*Our analysis indicates that the present statistics do not exclude severe violations of factorization and of the Vector Meson Dominance which are usually assumed in the literature*”.

One way to indirectly constrain the open-charm channel scenario would be through future, higher-statistics J/ψ measurements at GlueX, Hall-C, and SoLID. A direct alternative arises from the observation that the strength of the cusp structures and overall cross-sections in GlueX J/ψ data is related to the open-charm cross-sections, $\gamma p \rightarrow \bar{D}^0 \Lambda_c$, which Du *et al.* predict to range between one and two orders of magnitude higher than that of $\gamma p \rightarrow J/\psi p$, depending on model parameters, as depicted in the right panel of Figure 2. Therefore, one way to constrain the extent to which the open-charm exchange mechanism contributes to the total J/ψ cross-section is by measuring the open-charm cross-section itself, i.e. $\gamma p \rightarrow \bar{D}^0 \Lambda_c$ and $\gamma p \rightarrow \bar{D}^* \Lambda_c$. No previous measurement for open-charm photoproduction exists for photon energies below 20 GeV, making experiments at JLab 12 GeV rich in discovery potential.

The importance of directly measuring open-charm photoproduction near threshold has been emphasized in recent work, as evidenced by the following sample of quotes:

“*Since the strength of the cusps is connected to the rate for $\gamma p \rightarrow \bar{D}^0 \Lambda_c$, we also provide an estimate for the expected rate into the open-charm channels....measurements of the $\bar{D} \Lambda_c$ production will provide crucial information*”. Du *et al.* [21].

“*It is thus crucially important to constrain model parameters with further measurements in order to disentangle the possible physics scenarios and their implications...the measurement of open-charm photoproduction is needed to assess the role of coupled channels. A simultaneous analysis of the $\gamma p \rightarrow J/\psi$ and $\gamma p \rightarrow \bar{D}^0 \Lambda_c$ cross sections would provide a stringent constraint on the coupled channel dynamics. Based on the best fit parameters extracted here, we expect a large open-charm cross-section $\gtrsim 10$ nb. Furthermore, studies of photoproduction off nuclear targets may give further constrain on the total J/ψ -nucleon cross-section.*” Winney *et al.* (JPAC Collaboration) [22].

The cross-section for open-charm photoproduction near threshold is currently unknown, but measurements have been conducted at higher energies. The lowest-energy studies were performed at SLAC, where an experiment using a 20 GeV real photon reported a total open-charm cross-section of 56_{-24}^{+23} nb [23, 24]. Another SLAC study used a 10.5 GeV photon beam and reported an upper limit of 94 nb at a 90% confidence level [25]. The dominant channel for the energy range of interest is $\gamma p \rightarrow \bar{D}^0 \Lambda_c$, which is expected to dominate the total charm cross-section. The HERMES experiment also conducted searches for open-charm production in low-energy photoproduction, with unpublished measurements [26] of $D^{*\pm}$ production suggesting a total open-charm cross-section of:

$$[87.9_{-32.1}^{+40.7}(\text{stat}) \pm 9.2(\text{sys}) \pm 17.6(\text{frag. model})] \text{ nb at } E_\gamma = 15 \text{ GeV} \quad (1)$$

Tomasi-Gustafsson [27] predicts the $\gamma p \rightarrow \bar{D}^0 \Lambda_c$ cross-section to be approximately 40 nb at a photon energy of 10 GeV. As shown in Fig. 2, Du *et al.* predict an open-charm cross-section within the range of 50–100 nb for the 9–10 GeV range under one assumption, and 20–30 nb under an alternative set of model parameters. For comparison, the GlueX data reveals a $\gamma p \rightarrow J/\psi$ cross-section in the 9–10 GeV range that is approximately 0.3–1 nb (as shown in Figure 2).

II. EXPERIMENTAL SETUP

We envision taking advantage of the lifetime of the charmed hadrons by using a cut in the displaced vertex position relative to a thin target or prompt particles. The charmed mesons and baryons will travel $\mathcal{O}(100 \mu\text{m})$ before decaying. To measure this requires two key ingredients in our proposed experimental setup. The first is a thin target with a thickness not much greater than $100 \mu\text{m}$. The second requirement is we need to have a vertex resolution that is much smaller than the decay lengths. In the current CLAS12 setup, the vertex resolution is insufficient for this purpose. Instead, we will propose to borrow an existing detector, the MAPS Vertex tracker (MVTX) from the sPHENIX experiment, and insert it inside the CLAS12 Central Vertex Tracker. This displaced-vertex strategy is much more promising than relying solely on the CLAS12 PID systems, which would serve as the baseline for these searches but have limited momentum range and coverage. This possible detector setup is described in detail Sec. II A below, and we describe its integration in CLAS12 in Sec. II B.

A. The sPHENIX MAPS Vertex Tracker

sPHENIX is an ongoing experiment at RHIC [28], primarily dedicated to the study of quark-gluon plasma. At the heart of sPHENIX lies the Monolithic-Active-Pixel-Sensor (MAPS) vertex detector known as MVTX [29]. This detector is designed to track the vertices of particles generated from proton-proton and nucleus-nucleus collisions. More specifically, MVTX plays a crucial role in a physics program centered on the measurement of displaced vertices as signatures of heavy-quarks (charm and bottom) mesons and baryons. For reference, the single-track performance of MVTX within the 1.4 T solenoid field of sPHENIX is $40 \mu\text{m}$ for pointing resolution of distance-of-closest approach (DCA) for tracks with 0.5–1 GeV transverse momentum, and an efficiency of 80%.

The nominal layout of the MVTX in sPHENIX is defined with a barrel geometry, featuring an active length of 27 cm, with layer radial positions ranging from 22.4 to 42.1 mm. Its services are routed through a carbon-fiber cone structure from just one side of the detector. Figure 3 shows a picture of part of MVTX and services prior to installation in sPHENIX.

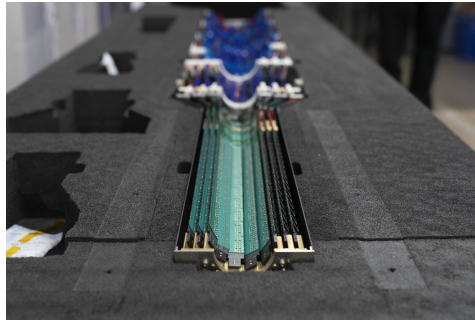


FIG. 3. Half of the sPHENIX MVTX detector and services prior to installation in sPHENIX. Figure credit: BNL/sPHENIX

B. Integration of the MVTX in CLAS12

We illustrate in Fig. 4 a potential layout for the MVTX within CLAS12, which would use the nominal geometry of the CLAS central trackers (CVT and FMT) and 5 T solenoid, as well as the nominal geometry of MVTX as used in sPHENIX. This layout would be possible by removing the vacuum chamber typically housing a cryotarget for liquid hydrogen or deuterium, thereby creating room for the MVTX detector and its associated services (which would be routed from only one side, as is done in sPHENIX). Instead of having a cryotarget, we would use a smaller vacuum chamber that could host a small solid target. The solid target system could be similar to those used in the CLAS12 run-group D or E experiments, which include several nuclear types in movable setup. The lightest solid target could be beryllium, while the heaviest could be lead or uranium oxide. For reference, the CLAS12 Silicon Vertex Tracker (SVT) inner-most layer is located at $r=65$ mm, and is enclosed by a Faraday cage. If we place the MVTX such that its upstream end is at the same z position as the solid target, as shown in Fig. 4, then the polar-angle acceptance of the MVTX is $8.7^\circ < \theta < 90^\circ$.

C. Trigger rate, radiation tolerance, material budget

The sPHENIX MVTX operates at a trigger rate of 15 kHz at RHIC, which is comparable to the CLAS12 DAQ rate. Additionally, the MAPS sensors have undergone radiation testing up to 2 Mrad, exceeding the anticipated doses from the sPHENIX program, and no radiation damage is expected [29], neither during CLAS12 operation. On the other hand, the hit occupancy at CLAS12 would be much smaller compared to RHIC running. Given the MVTX's material budget is less than $< 0.5\%X_0$ per layer, we expect no detrimental impact on the CLAS12 CVT performance.

D. Triggering with the Forward Tracker

Possible triggers could be implemented using the forward tagger (FT), which was designed to measure small-angle scattering to access the the small- Q^2 regime of electro-production ($0.01 < Q^2 < 0.1$). Nominally, the kinematic range

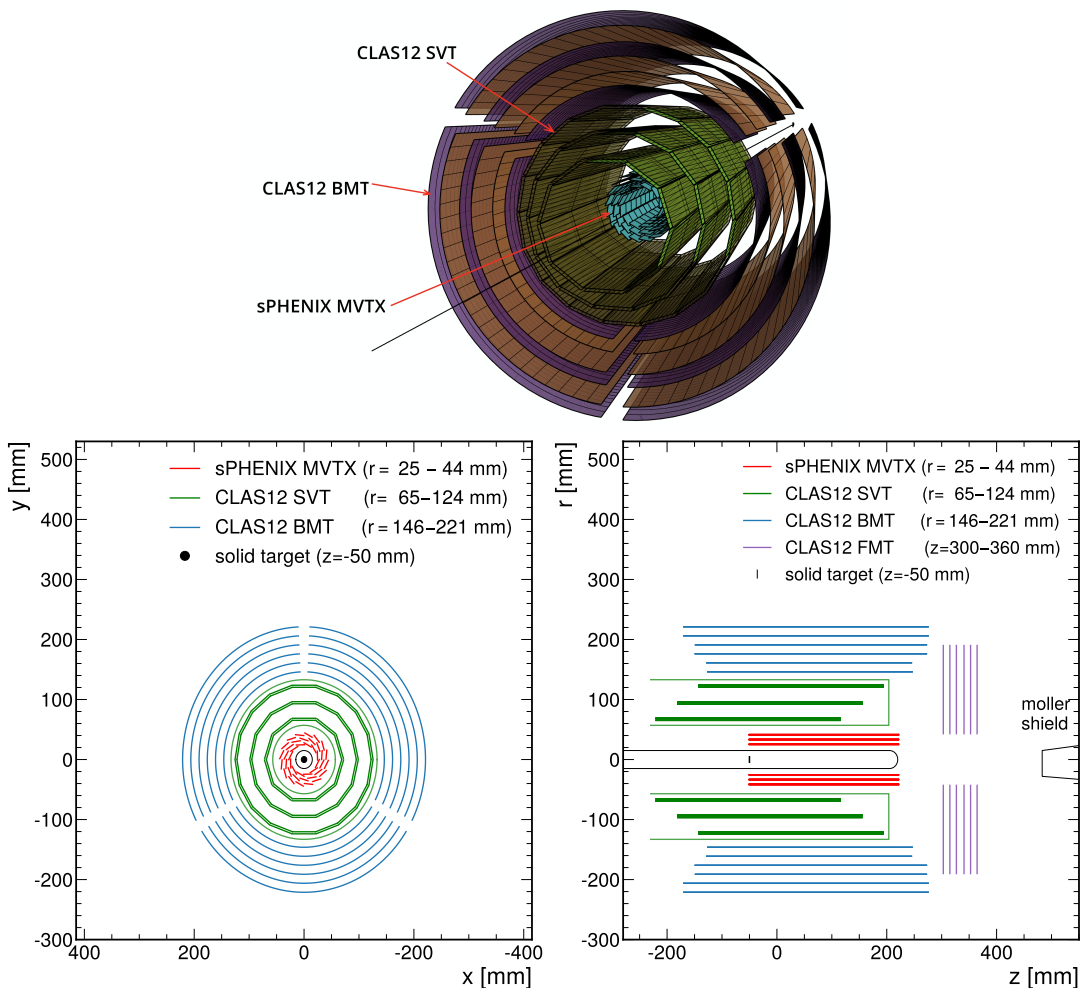


FIG. 4. Top: Rendering of possible layout of sPHENIX MVTX (cyan) with the CLAS12 SVT (green) and BMT (purple and orange). Bottom: Possible layout of the sPHENIX MVTX and the CLAS12 SVT and BMT. This configuration would be compatible with a solid-target.

of the FT is $2.5^\circ < \theta < 4.5^\circ$ for the polar angle [30] and it has an energy range of 0.5 to 4.5 GeV. Therefore, the virtual-photon energy range in this proposed experiment is bound from above by the beam energy minus the minimum energy detectable for the scattered electron, and from below by the $\Lambda_c^+ \bar{D}^0$ threshold. That is, $8.7 < \nu < 10.1$ GeV.

III. OBSERVABLES AND ANALYSIS METHODS

The physics observable in this analysis will be the cross section of the $\gamma^* p \rightarrow \Lambda_c^+ \bar{D}^{(*)0}$ reaction. We will not distinguish in this analysis between events in which the \bar{D}^0 is directly produced and those in which it is from the decay of a \bar{D}^{*0} . If the measured cross section is large enough, we will divide our data sample into bins in the virtual photon energy, ν .

To measure these cross sections, we will select events with a scattered electron in the FT and candidate of the following charmed hadron decay modes:

$$\Lambda_c^+ \rightarrow K^- \pi^+ p \text{ (B.R.} = 6.28 \pm 0.32\%), \quad (2)$$

and

$$\bar{D}^0 \rightarrow K^+ \pi^- \text{ (B.R.} = 3.88 \pm 0.05\%). \quad (3)$$

We choose these decays modes because they have a small number of total particles in the final state, all of which are charged, and have relatively large branching ratios.

To reduce background, we will require a cut on the z position of the decay vertex of the charmed-hadron candidate, v_z , as obtained using the MVTX¹. We will further reduce background by using a ‘‘bump-hunt’’ technique on the invariant-mass distribution of the remaining candidates. That is, we will fit this distribution to a polynomial (representing any background that remains after the displaced-vertex cut) plus a Gaussian (representing the signal from the charmed particle decay).

The cross section will then be determined as

$$\sigma_{\gamma p \rightarrow \Lambda_c^+ \bar{D}^{(*)0}} = \frac{N_{\text{fit}}}{\ell f_{ep/\gamma p} \epsilon} \quad (4)$$

where N_{fit} is the signal yield from the polynomial+Gaussian fit, ℓ is the luminosity, $f_{ep/\gamma p}$ is the conversion factor from quasi-real photoproduction² to real photoproduction, and ϵ is the overall detection efficiency (which includes acceptance effects, detector efficiency, and event-selection cuts) which will be determined using Monte-Carlo simulations.

IV. ESTIMATED REACH

In this section, we provide a rough estimation of the experimental reach for the proposed measurement. These estimates will need to be further refined by future studies using Geant simulations and existing CLAS12 data.

A. Total expected cross section

Du *et al.* predicted the cross sections for the $\Lambda_c^+ \bar{D}^0$ and $\Lambda_c^+ \bar{D}^{*0}$ and presented the results in Ref. [21] with two different values of the model parameter η . These two estimates of the cross section differ by a factor of ≈ 4 . We consider the lower estimate of the cross section (corresponding to $\eta = 0.5$) to be more realistic, because it is consistent with the experimental upper limit of 94 nb at a 90% confidence level for total charm production determined by SLAC with a 10.5 GeV photon beam [25]. For comparison, the sum of the cross sections for \bar{D}^0 and \bar{D}^{*0} channels in Du. *et al.* is about 90 nb. We will therefore base our estimates here on the $\eta = 0.5$ calculations.

The cross section for quasi-photoproduction (that is, electro-production with $Q^2 \approx 0$) is related to that of real photoproduction by

$$\sigma_{ep} = \int_{y_{\text{min}}}^{y_{\text{max}}} \frac{\alpha}{\pi y} \sigma_{\gamma p}(\nu) \left((1 - y + 1/2y^2) \log \left(\frac{Q_{\text{max}}^2}{Q_{\text{min}}^2} \right) + m_e^2 y^2 (Q_{\text{max}}^{-2} - Q_{\text{min}}^{-2}) \right) \quad (5)$$

where $y = \nu/E_{\text{beam}}$, y_{min} is evaluated at the threshold value of ν and y_{max} is determined by the minimum detectable scattered-electron energy. The limits on Q^2 for a given y are given by $4E_{\text{beam}}^2(1-y)\sin^2\theta_{\text{min}}^e$ and $4E_{\text{beam}}^2(1-y)\sin^2\theta_{\text{max}}^e$, where the limits on θ_e are determined by the acceptance of the FT (2.5° to 4.5°).

This evaluates to ≈ 0.0046 nb with \bar{D}^0 and ≈ 0.0036 nb with \bar{D}^{*0} , which combined is ≈ 0.0082 nb.

Since similar reactions on neutrons (*e.g.* $\gamma n \rightarrow \Lambda_c^+ D^-$) are expected to be at least an order of magnitude less than those on protons [27], the per-nucleon cross section would be about Z/N times smaller than the free-proton cross-section. This evaluates to a factor of $4/9 \approx 0.44$ for ${}^9\text{Be}$.

B. Luminosity

To provide ample luminosity while simultaneously preventing the target foil from being so thick that charmed hadrons would decay before exiting the target, we could use a multi-foil target, as was done in Run-Group M with a multi-foil carbon target. Using a 5-foil Be target with 100 μm for each foil and an 85 nA beam would correspond to $3.0 \times 10^{34} \text{ cm}^{-2}\text{s}^{-1}$. For reference, in the currently-running Run-Group E experiment at CLAS12, the luminosity for solid-target production runs are $1.0 \times 10^{35} \text{ cm}^{-2}\text{s}^{-1}$ for carbon (1.5 mm thick foil at 85 nA) and $4.3 \times 10^{34} \text{ cm}^{-2}\text{s}^{-1}$ for lead (143 μm thick target with 70 nA).

100 days of running at $3.0 \times 10^{35} \text{ cm}^{-2}\text{s}^{-1}$ and PAC efficiency of 50% corresponds to $1.62 \times 10^8 \text{ nb}^{-1}$ of luminosity. Multiplying this by the cross sections in the previous section (and including a factor of 0.44 for the proton fraction) yields $\approx 270\text{k}$ $\Lambda_c^+ \bar{D}^0$ events and $\approx 210\text{k}$ $\Lambda_c^+ \bar{D}^{*0}$ events, which combined is $\approx 470\text{k}$ events.

¹ As an alternative, if there are also prompt particles measured in this reaction, it may be possible to cut on the difference in v_z between the prompt particles and the displaced vertex.

² That is, ep scattering at low Q^2

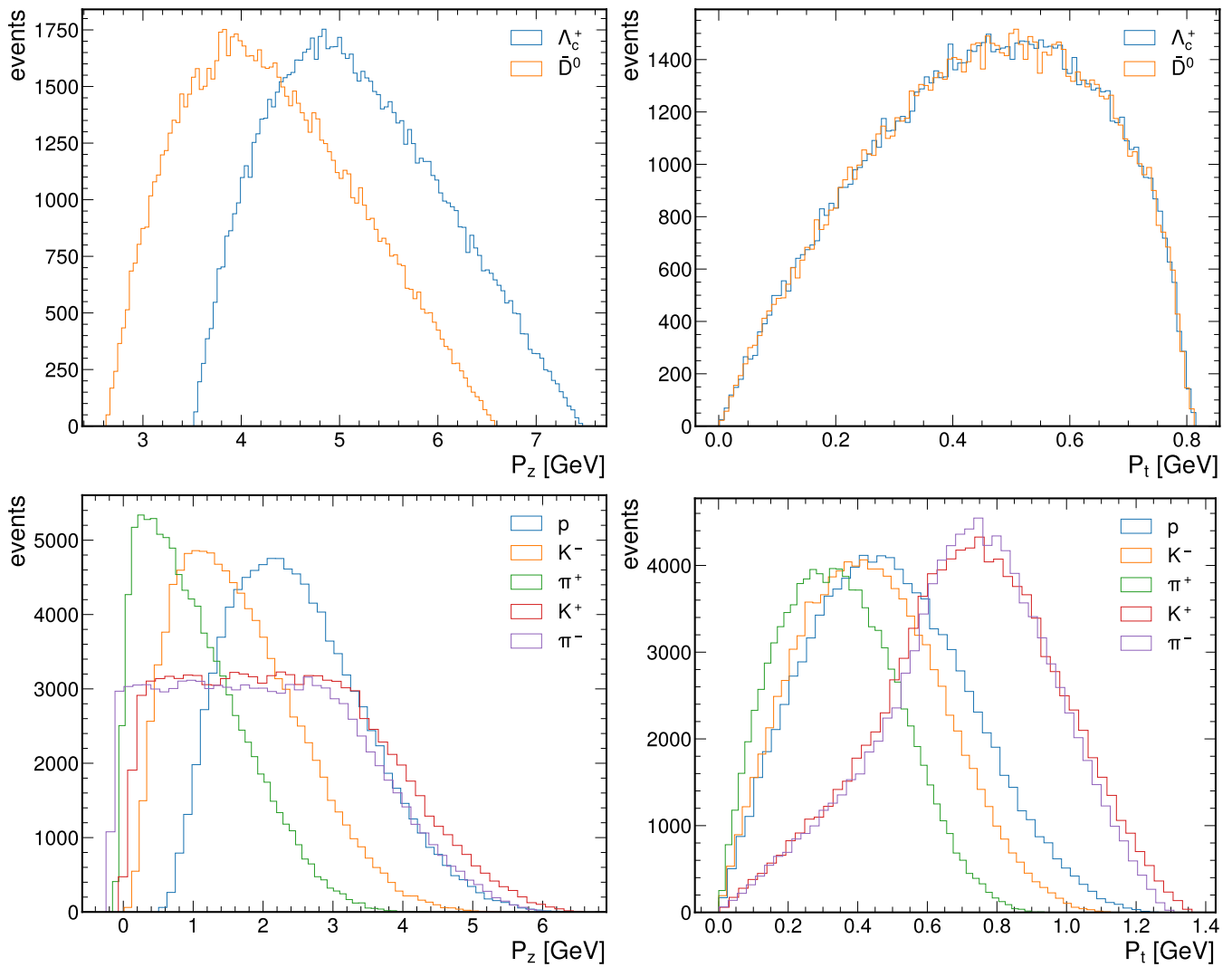


FIG. 5. Top row: longitudinal (left) and transverse (right) momenta distributions for the generated charmed hadrons. Bottom row: same, for their daughter particles

C. Monte-Carlo Simulations

To estimate the number of events in which either the Λ_c^+ or \bar{D}^0 can be measured through their decays, we first ran MC simulations of $ep \rightarrow e'\Lambda_c^+\bar{D}^0$ channel, in which the electron kinematic distributions correspond to Eq. 5. The $\Lambda_c^+\bar{D}^0$ pairs were then produced with a uniform distribution in phase space given the combined four momentum of the virtual photon and proton. We then allowed the simulated \bar{D}^0 to decay isotropically into a $K^+\pi^-$ pair, with the vertex-position given by an exponential distribution, taking into consideration the lifetime of the \bar{D}^0 and time dilation. We did the same for the Λ_c^+ , with the $K^-\pi^+p$ being generated with uniform probability within the 3-particle phase space. The resulting momentum distributions for these simulated events are shown in Fig. 5.

D. Estimation of efficiency and acceptance

Assuming that there is a combined detection efficiency and acceptance of around 80% for each of the hadrons in the forward detector, and a similar efficiency for the electrons in the FT, approximately $(80\%)^3 \approx 52\%$ ($(80\%)^4 \approx 41\%$) of the events with $e'K^+\pi^-$ ($e'K^-\pi^+p$) in their final state will have all of these particles reconstructed. We will further refine these estimates of the event-reconstruction with using CLAS12's detector-response simulator package, GEMC.

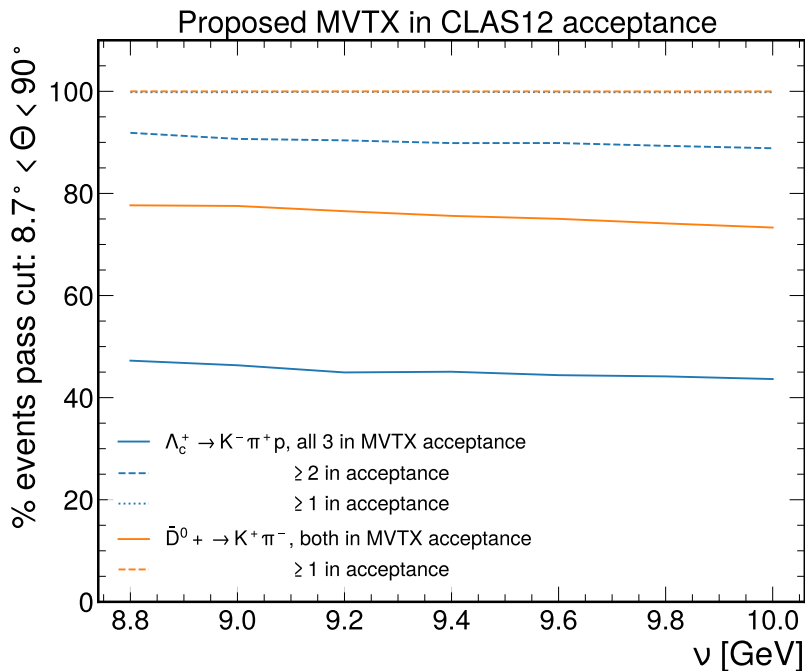


FIG. 6. Overall geometric acceptance of the MVTX for detecting at least one of the daughter particles (dashed curves), at least two daughter particles (dotted curves) and all of the daughter particles (solid curves) for Λ_c^+ (blue) and \bar{D}^0 (orange).

E. Geometric acceptance of the MVTX

To estimate the acceptance of the MVTX, we used the generated event sample described above. In principle, determining the decay position of a charmed hadron requires at least one of its decay products to be within the proposed, nominal acceptance of MVTX at CLAS12: $8.7^\circ < \theta < 90^\circ$. However, as an alternative to reduce backgrounds from poorly reconstructed single tracks, it is possible to require at least two of the decay products to be reconstructed in the MVTX, or in the case of the Λ_c^+ decay, all three of the daughter particle candidates. We show the overall geometric acceptance of the MVTX (that is the fraction of the generated events which a requisite number of the decay products are in the MVTX's geometric acceptance) of each of these scenarios in Fig. 6. Almost all of the events have at least one daughter particle in the MVTX's acceptance. Even in the most strict requirements (requiring all three daughter particles from the Λ_c^+ in the MVTX acceptance) would retain over 40% of the events.

F. MVTX efficiency

We estimate an 80% efficiency for reconstructing each daughter particle in the MVTX, leading to $(80\%)^3 \approx 51\%$ efficiency for the $K^-\pi^+p$ decay and $(80\%)^3 \approx 64\%$ for the $K^+\pi^-$ channel, for events where all of the daughter particles are in the geometric acceptance of the MVTX. A more precise estimate of this efficiency can be determined through future studies with Geant simulations.

G. Event retention after displaced-vertex cut

To estimate how the thickness of the target would affect the efficiency of a displaced-vertex cut, we used the event-generator simulations described above. The resolution for the vertex position of a track can depend on several factors including the magnetic field, the polar angle of the track, and the transverse momentum of the particle. This will need to be determined through further studies with Geant simulations. In this exercise, we choose to use a conservative cut on v_z at $250 \mu\text{m}$ from the downstream face of the target foil. The efficiency of this cut can be calculated as:

$$\epsilon_h(v_{z,\text{cut}}) = \frac{N(v_z^h > v_{z,\text{cut}})}{N_{\text{tot}}} \quad (6)$$

where $N(v_z > v_{z,\text{cut}})$ is the number of events where the reconstructed decay position of one of the charmed hadrons, v_z^h , (where the h index represents either Λ_c^+ or \bar{D}^0), is greater than the cutoff, $v_{z,\text{cut}}$. The v_z^h for each event is given by

$$v_z^h = v_z^{h,\text{gen}} + v_z^e \quad (7)$$

where $v_z^{h,\text{gen}}$ is the z position of the charmed-hadron decay from the event generator (*i.e.*, relative to the electron vertex), and v_z^e is the electron vertex, which assigned uniformly to each event between $-t$ and 0 , where t is the thickness of the foil.

The resulting cut efficiency, as a function of the foil thickness, is shown in Fig. 7. With 100 μm foils, about 12% of Λ_c^+ s and 34% of \bar{D}^0 s decay after the cutoff. For reference, the CLAS12 run-group E experiment (on-going at the time of writing this letter of intent) uses a Pb target that is 143 μm thick.

We intend to follow up these estimates with more refined tracking studies using realistic field maps provided by the CLAS12 magnet and Kalman-Filter reconstruction.

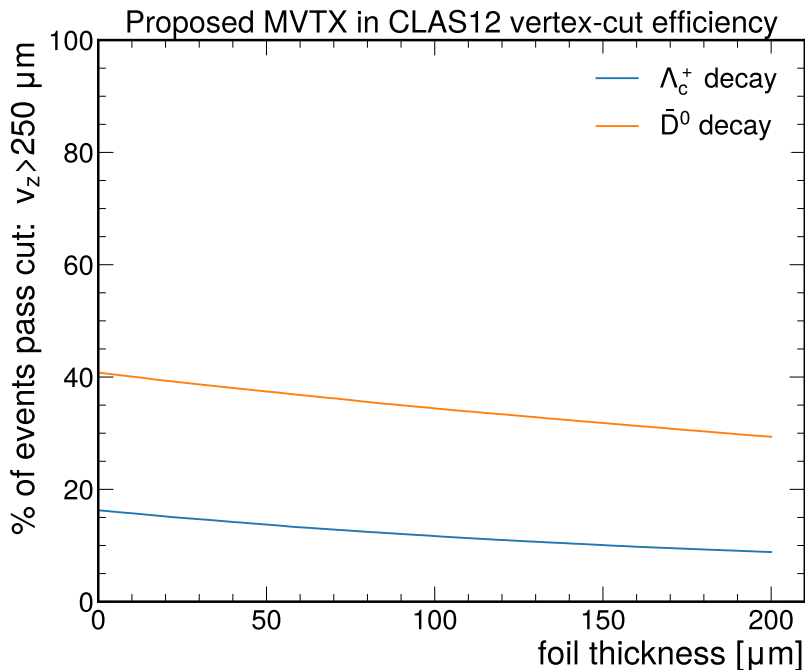


FIG. 7. Efficiency for a displaced-vertex cut at 250 μm for the Λ_c^+ (blue) and \bar{D}^0 (orange) channels respectively. For reference, the expected distance these particles travel is 130 (260) μm for Λ_c^+ (\bar{D}^0) at the mode energy, 4.9 (3.9) GeV.

H. Expected sample size and reach

To estimate the number of events that can be measured for a given sample, we multiplied the total number of expected events by the branching ratio for a given channel, times the CLAS12 overall efficiency, the geometric acceptance of the MVTX, and the event retention rate of the displaced vertex cut, as detailed in the previous subsections. This yields, as a conservative estimate, 340 events with a reconstructed Λ_c^+ candidate and 1.6k events with a \bar{D}^0 candidate. The factors that go into these calculations are summarized in Table I.

We have not studied background rates, as it heavily relies upon the background-rejection power of the vertex-position cuts, which requires detailed tracking studies with Geant simulations. These are outside the scope of this Letter of Intent.

Quantity	$K^- \pi^+ p$	$K^+ \pi^-$	notes
free-proton cross-section	0.0082 nb		$\sigma_{\gamma p}$ calculated from Ref. [21], $\eta = 0.5$, converted to σ_{ep} (Eq. 5)
Z/N	0.44		evaluated for ${}^9\text{Be}$
Tot. luminosity	1.3×10^8 nb $^{-1}$		100 days, 50% PAC efficiency, 10^{35} cm $^{-2}$ s $^{-1}$, achieved with 5-foil, 100 μm Be target at 85 nA; evaluated per nucleon
Branching ratio	6.26%	3.88%	from PDG
CLAS12 efficiency	41%	51%	assuming 80% per detected particle
MVTX acceptance	45%	76%	all daughter particles in MVTX
MVTX efficiency	51%	64%	assume 80% reconstruction efficiency per daughter particle
v_z cut	12%	34%	assuming 100 μm per foil, 250 μm cut
Tot. expected signal events	340	1600	

TABLE I. Factors and assumptions that go into the calculations for the total expected yields (bottom row).

V. SUMMARY AND CONCLUSIONS

The inclusion of measurements on open-charm production at JLab would complement the existing J/ψ program, offering valuable insights into reaction mechanisms. Direct measurements of channels such as $\gamma p \rightarrow \bar{D}^0 \Lambda_c$ and $\gamma p \rightarrow \bar{D}^* \Lambda_c$ would contribute to constraining the J/ψ reaction mechanisms, shedding light on whether the open-charm coupled channel mechanism [21] plays a significant role in the observed J/ψ cross-sections. This constraint is crucial for a nuanced interpretation of J/ψ data, challenging the commonly used vector-meson dominant model employed for extracting gravitational form factors of the nucleon.

To execute this program, the conclusion of operations for sPHENIX MVTX post-RHIC shutdown offers a promising opportunity. Using its capability to offer clear D-meson tagging via displaced vertex signatures, we suggest incorporating the sPHENIX MVTX geometry into the CLAS12 tracker. This integration, dependent on removing the standard vacuum scattering chamber and cryotarget, would involve installing a smaller vacuum chamber to accommodate a small solid target that would consist of multiple foils each $\approx 100 \mu\text{m}$ thick.

The use of light solid targets like beryllium or carbon, with appropriate modeling, holds the potential to constrain corresponding cross-sections on a proton target. Additionally, an inclusive D-meson production program with light and heavy nuclear targets such as lead or uranium-oxide could provide insights into cold-nuclear matter effects with charm quarks, which could complement ongoing light-quark studies at JLab [31, 32]. All of these could complement and pave the way for proposed charm studies at the Electron-Ion Collider [33] and JLab at 22 GeV [34].

We intend to follow up this LOI with detailed Geant detector simulations, encompassing signals and backgrounds, as well as thorough technical assessments of operating conditions in CLAS12, or other detector at JLab.

-
- [1] D. Kharzeev, H. Satz, A. Syamtomov, and G. Zinovjev, J/ψ photoproduction and the gluon structure of the nucleon, *Eur. Phys. J. C* **9**, 459 (1999), arXiv:hep-ph/9901375.
 - [2] S. J. Brodsky, E. Chudakov, P. Hoyer, and J. M. Laget, Photoproduction of charm near threshold, *Phys. Lett. B* **498**, 23 (2001), arXiv:hep-ph/0010343.
 - [3] K. A. Mamo and I. Zahed, Diffractive photoproduction of J/ψ and Υ using holographic QCD: gravitational form factors and GPD of gluons in the proton, *Phys. Rev. D* **101**, 086003 (2020), arXiv:1910.04707 [hep-ph].
 - [4] Y. Guo, X. Ji, and Y. Liu, QCD Analysis of Near-Threshold Photon-Proton Production of Heavy Quarkonium, *Phys. Rev. D* **103**, 096010 (2021), arXiv:2103.11506 [hep-ph].
 - [5] D. E. Kharzeev, Mass radius of the proton, *Phys. Rev. D* **104**, 054015 (2021), arXiv:2102.00110 [hep-ph].
 - [6] K. A. Mamo and I. Zahed, J/ψ near threshold in holographic QCD: A and D gravitational form factors, *Phys. Rev. D* **106**, 086004 (2022), arXiv:2204.08857 [hep-ph].
 - [7] X.-Y. Wang, F. Zeng, and Q. Wang, Gluon gravitational form factors of protons from charmonium photoproduction*, *Chin. Phys. C* **47**, 074101 (2023), arXiv:2208.03186 [hep-ph].
 - [8] Y. Guo, X. Ji, Y. Liu, and J. Yang, Updated analysis of near-threshold heavy quarkonium production for probe of proton's gluonic gravitational form factors, *Phys. Rev. D* **108**, 034003 (2023), arXiv:2305.06992 [hep-ph].
 - [9] J. Dudek *et al.*, Physics Opportunities with the 12 GeV Upgrade at Jefferson Lab, *Eur. Phys. J. A* **48**, 187 (2012), arXiv:1208.1244 [hep-ex].
 - [10] S. Joosten and Z. E. Meiziani, Heavy Quarkonium Production at Threshold: from JLab to EIC, *PoS QCDEV2017*, 017 (2018), arXiv:1802.02616 [hep-ex].
 - [11] A. Ali *et al.* (GlueX), First Measurement of Near-Threshold J/ψ Exclusive Photoproduction off the Proton, *Phys. Rev. Lett.* **123**, 072001 (2019), arXiv:1905.10811 [nucl-ex].

- [12] S. Adhikari *et al.* (GlueX), Measurement of the J/ψ photoproduction cross section over the full near-threshold kinematic region, *Phys. Rev. C* **108**, 025201 (2023), [arXiv:2304.03845 \[nucl-ex\]](#).
- [13] B. Duran *et al.*, Determining the gluonic gravitational form factors of the proton, *Nature* **615**, 813 (2023), [arXiv:2207.05212 \[nucl-ex\]](#).
- [14] J. Newton, *J/ψ Photoproduction Near Threshold With CLAS12*, Ph.D. thesis, Old Dominion U. (main), Old Dominion U. (2021).
- [15] R. Tyson, *J/ψ Near-Threshold Photoproduction off the Proton and Neutron with CLAS12*, Ph.D. thesis, University of Glasgow, Glasgow U. (2023).
- [16] J. Arrington *et al.* (Jefferson Lab SoLID), The solenoidal large intensity device (SoLID) for JLab 12 GeV, *J. Phys. G* **50**, 110501 (2023), [arXiv:2209.13357 \[nucl-ex\]](#).
- [17] O. Gryniuk and M. Vanderhaeghen, Accessing the real part of the forward J/ψ -p scattering amplitude from J/ψ photoproduction on protons around threshold, *Phys. Rev. D* **94**, 074001 (2016), [arXiv:1608.08205 \[hep-ph\]](#).
- [18] I. Strakovsky, D. Epifanov, and L. Pentchev, J/ψ p scattering length from GlueX threshold measurements, *Phys. Rev. C* **101**, 042201 (2020), [arXiv:1911.12686 \[hep-ph\]](#).
- [19] L. Pentchev and I. I. Strakovsky, J/ψ -p Scattering Length from the Total and Differential Photoproduction Cross Sections, *Eur. Phys. J. A* **57**, 56 (2021), [arXiv:2009.04502 \[hep-ph\]](#).
- [20] X.-Y. Wang, F. Zeng, and I. I. Strakovsky, $\psi^{(*)}$ p scattering length based on near-threshold charmonium photoproduction, *Phys. Rev. C* **106**, 015202 (2022), [arXiv:2205.07661 \[hep-ph\]](#).
- [21] M.-L. Du, V. Baru, F.-K. Guo, C. Hanhart, U.-G. Meißner, A. Nefediev, and I. Strakovsky, Deciphering the mechanism of near-threshold J/ψ photoproduction, *Eur. Phys. J. C* **80**, 1053 (2020), [arXiv:2009.08345 \[hep-ph\]](#).
- [22] D. Winney *et al.* (Joint Physics Analysis Center), Dynamics in near-threshold J/ψ photoproduction, *Phys. Rev. D* **108**, 054018 (2023), [arXiv:2305.01449 \[hep-ph\]](#).
- [23] K. Abe *et al.* (SLAC Hybrid Facility Photon), CHARM PHOTOPRODUCTION AT 20-GeV, *Phys. Rev. D* **30**, 1 (1984).
- [24] K. Abe *et al.*, CHARM PHOTOPRODUCTION CROSS-SECTION AT 20-GeV, *Phys. Rev. Lett.* **51**, 156 (1983).
- [25] K. Abe *et al.* (SLAC Hybrid Facility Photon), Search for a Threshold Enhancement in the $\gamma(p) \rightarrow$ Charmed Baryon + Charmed Meson Cross-section, *Phys. Rev. D* **30**, 694 (1984).
- [26] E. Volk, *Measurement of the $D^{*\pm}$ cross-section at HERMES*, Ph.D. thesis, Hamburg U. (2001).
- [27] E. Tomasi-Gustafsson, Charm production in NN and γN collisions, in *17th International Baldin Seminar on High Energy Physics Problems: Relativistic Nuclear Physics and Quantum Chromodynamics*, Vol. V2 (2005) pp. 231–240, [arXiv:hep-ph/0411295](#).
- [28] A. Adare *et al.* (PHENIX), An Upgrade Proposal from the PHENIX Collaboration, (2015), [arXiv:1501.06197 \[nucl-ex\]](#).
- [29] Ming Liu *et al.*, A Monolithic-Active-Pixel-Sensor-based Vertex Detector (MVTX) for the PHENIX Experiment at RHIC”, proposal submitted to DOE Office of Science, <https://www.phenix.bnl.gov/WWW/publish/barish/publish/mxliu/sPHENIX/MVTX-Project/MVTX-Preproposal-v1.5-02012017.pdf>.
- [30] A. Acker *et al.*, The CLAS12 Forward Tagger, *Nucl. Instrum. Meth. A* **959**, 163475 (2020).
- [31] S. Moran *et al.* (CLAS), Measurement of charged-pion production in deep-inelastic scattering off nuclei with the CLAS detector, *Phys. Rev. C* **105**, 015201 (2022), [arXiv:2109.09951 \[nucl-ex\]](#).
- [32] S. J. Paul *et al.* (CLAS), Observation of Azimuth-Dependent Suppression of Hadron Pairs in Electron Scattering off Nuclei, *Phys. Rev. Lett.* **129**, 182501 (2022), [arXiv:2207.06682 \[nucl-ex\]](#).
- [33] A. Accardi *et al.*, Electron Ion Collider: The Next QCD Frontier: Understanding the glue that binds us all, *Eur. Phys. J. A* **52**, 268 (2016), [arXiv:1212.1701 \[nucl-ex\]](#).
- [34] A. Accardi *et al.*, Strong Interaction Physics at the Luminosity Frontier with 22 GeV Electrons at Jefferson Lab, (2023), [arXiv:2306.09360 \[nucl-ex\]](#).